UNIVERSAL MODELLING AND ANALYSIS OF GRID-SCALE ELECTROLYSERS FREQUENCY RESPONSE IN WIND-DOMINATED POWER SYSTEMS

Long Phan-Van[1, 2], Van Nguyen Dinh[2, 3], Tuyen Nguyen-Duc[1*]

[1]Department of Electrical Engineering, Hanoi University of Science and Technology, Hanoi, Vietnam
[2]OWC, ABL Group, Ho Chi Minh City, 700000, Vietnam
[3]OWC, ABL Group, Cork, T12 W7CV, Ireland

Keywords: ELECTROLYSER, FREQUENCY RESPONSE, RENEWABLE ENERGY SOURCES, DEMAND-SIDE RESPONSE

Abstract

Integrating hydrogen technologies such as electrolysers could provide frequency support to renewable energy-dominated power systems while also ensuring the production of green hydrogen. This study aims to improve the frequency performance of wind-dominated power systems by investigating the implementation of grid-scale electrolyser plants to provide frequency stability support. Firstly, a universal system frequency response (SFR) model is proposed, which allows for high accuracy compared to the full-order model and requires low computation time. The electrolyser plant power-tracking response model and its proposed control strategies for frequency regulation are then integrated into this improved SFR model. Finally, a modified IEEE 39-bus system with 50% wind penetration is used to evaluate the capability of large-scale electrolyser plants to provide frequency support using different control strategies and electrolyser types. It is found that the proposed RoCoF-based droop control and virtual inertia controller can significantly improve the system frequency response during an extreme power disturbance. Additionally, due to its slow response characteristic, the alkaline electrolyser plant negatively impacts the electrolyser plant frequency support ability.

1. Introduction

The transition towards renewable energy sources (RES) due to energy decarbonisation and sustainability goals has resulted in increased penetration of RES around the globe, with the total capacity reaching 3,372 GW at the end of 2022 [1]. However, operating a RES-dominated power system might present several challenges, one of which is the lack of inertia due to reduced rotational inertia share from traditional synchronous generators (SGs), which can result in poor grid frequency response during extreme power disturbances, leading to possible operational issues such as tripping of generating units and under-frequency load-shedding [2]. To ensure frequency stability within the power grid, system operators have procured frequency ancillary services from both generators and demands. Among all the available options, water electrolysis is an eco-friendly technology that can speed up the decarbonisation of energy systems in the future, while also offering frequency regulation services. Its ability to regulate to full load within seconds has been proven in past experiments [3], making this technology appropriate for supplying frequency regulation to power grids. In the past, studies that relate to grid-connected electrolysers have primarily focused on optimal planning [4] [5], energy management [6] [7], and techno-economic evaluation [8] [9] of hydrogen-based energy systems, without considering too much on the problem of electrolyser support in frequency regulation in lower inertia power systems.

In recent years, more work has been carried out to investigate this problem. Aiming to evaluate how grid-scale electrolysers could support a RES-dominated power system under extreme disturbance, authors in [10] have proposed a detailed dynamic model to study fast frequency response from large-scale electrolysers. In addition, the impacts of stack voltage-current nonlinear characteristics on the fast frequency response capability of large-scale electrolysers are also studied and discussed in [11]. In [12], the authors focused on researching the capabilities of hydrogen electrolysers to provide virtual inertia and primary and secondary frequency response. The impacts of the response time of different electrolyser types and other hydrogen production constraints on the frequency response capability of the electrolyser are also studied. In the three studies above, the simplified model of the Australian multi-area power system with 50% renewables is used to run different case studies for evaluation. The authors in [13] focus on investigating the analytical evaluation and integration of large-scale alkaline electrolyser plants into power systems to provide frequency support. Additionally, the study also gives an economic analysis of the profitability of alkaline electrolysers providing frequency support. Another study that focused on using proton exchange membrane (PEM) electrolysers to ensure power system frequency stability is presented in [14], using numerical studies to validate the efficiency of its proposed models.

Overall, previous research requires significant knowledge of control theory for detailed dynamic model simulation [10] [11] [12] [13], and a high number of input parameters for transfer function-based system frequency response (SFR) model simulation [14]. Thus, a universal SFR model that allows high accuracy and fast computation, while requiring low effort to generate the initial input parameters, compared to full model time-domain simulation, is needed. Additionally, an in-depth

analysis of the electrolyser plants' ability to provide frequency support for RES-dominated power systems needs to be further developed, focusing on analysing different electrolysis technologies and control strategies.

To bridge such research gaps indentified in the previous studies, this study aims to conduct a comprehensive analysis of the frequency support capability of grid-scale electrolyser plants in wind-dominated power systems, considering different control strategies and response characteristics of PEM and alkaline electrolysers. The classical SFR model used for frequency stability studies is also improved by using the particle swarm optimisation (PSO) algorithm, ensuring high accuracy and low computation burden. The original contributions of this work are summarised as follows:

- Propose a universal system frequency response model that allows high accuracy and fast computation, compared to full model time-domain simulation.
- Introduce three active power-frequency (P-f) control strategies for the electrolyser plant to study their abilities in frequency stability support, including virtual inertia response and primary frequency response.
- Compare the impacts of the power-tracking response characteristics of the PEM and alkaline electrolyser plants on the ability to provide frequency support.
- Carry out case studies in the modified IEEE 39-bus system with 50% wind turbine penetrated.

2. Universal System Frequency Response Model

2.1. *Classical SFR Model*

In a conventional power grid model, the swing equation of synchronous generators and frequency-dependent loads are responsible for regulating the frequency response of the system. By applying these two swing equations to a disturbance, the SFR can be described as [15]:

$$\frac{d\Delta f}{dt} = \frac{1}{2H_{sys}} \times \left[\Delta P_m - \left(\Delta P_L + D\Delta f\right)\right] \quad (1)$$

where Δf is the frequency deviation of the power grid; ΔP_m is the change in SGs mechanical power output caused by frequency disturbance; ΔP_L is the change in frequency-independent loads' consumed power; D is the system damping constant which represents the frequency-dependency of loads that can respond to frequency disturbance; and H_{sys} represents the equivalent inertia constant of the power grid.

The swing equation is described in Figure 1, which includes two feedback loops: (1) the prime-mover model (described by a simplified steam or hydraulic turbine model) and (2) the load frequency-dependency model (described by a static droop coefficient). It can be seen that the classic SFR model only applies to power systems with thermal or hydropower plants and does not consider the presence of controllable loads.

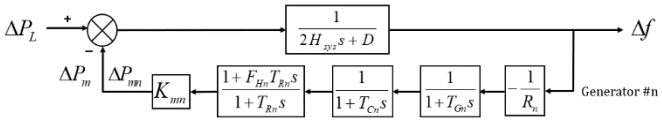

Figure 1 Classical multi-machine SFR model

2.2. *Modified SFR Model*

Using the classical SFR model for modern power systems is problematic since the model only takes into account steam or hydraulic turbines, which may not be appropriate for RES-dominated power systems [16]. In addition, the classical SFR model requires a large number of initial parameters that can be hard to identify. Finally, the classical model does not consider the impacts of fast-responding loads such as grid-scale electrolyser plants.

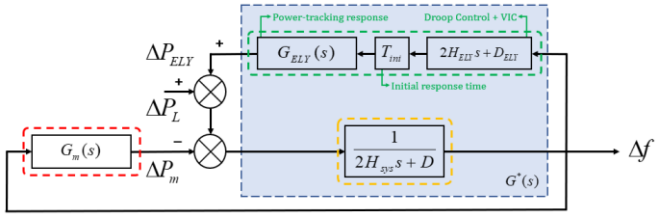

Figure 2 Modified SFR model

In order to overcome the first and second challenges mentioned above, which is having multiple power sources integrated into the power grid, as well as to increase model accuracy, and limit the use of complicated prime-mover models with hard-to-identify parameters, this paper utilises a generic third-order transfer function $G_m(s)$ to describe the equivalent dynamics of the aggregate prime mover generators (Eq. (2)), inspired by [16]. The modified SFR model is presented in Figure 2. Based on the power disturbance and the frequency response obtained from a real power grid or detailed model, the parameters of the generic model (X, H and D) can be identified by using fitting methods. In this study, we proposed a PSO-based method to estimate the required parameters, with the objective of minimising the root-mean-square error (RMSE) of the frequency response between the proposed SFR model and the detailed model simulated in the PSS/E software. The fitting algorithm and the equation for RMSE are presented later in Section 4.1.

$$G_m(s) = \frac{x_1 s^2 + x_2 s + x_3}{x_4 s^2 + x_5 s + x_6 + 1} \quad (2)$$

In order to overcome the third challenge, an electrolyser plant dynamic frequency regulation model is integrated into the modified SFR model, which includes a droop controller and a virtual inertia controller (VIC) that generate the reference power consumption according to the system frequency, as well as a power-tracking response model that describes the power response characteristic of the electrolyser plant (PEM and Alkaline). The active power-frequency characteristics, generated by the droop controller and VIC, can be derived as:

$$\frac{d\Delta f}{dt} = \frac{1}{2H_{vir}} \times \left[\Delta P_{ELY}^{ref} - D_{ELY}\Delta f\right] \quad (3)$$

where H_{vir} and D_{ELY} are the virtual inertia and droop coefficient of the electrolyser plant, and ΔP_{ELY}^{ref} is the reference power of the electrolyser plant, which can be identified using Eq. (4).

$$\Delta P_{ELY}^{ref}(s) = \left(D_{ELY} + 2H_{vir}s\right) \times \Delta f(s) \quad (4)$$

The reference power consumption of the electrolyser plant, created by the controllers, is then fed into the first-order model $G_{ELY}(s)$, which emulates the electrolyser plants' power-tracking response, as shown in Eq. (5).

$$G_{ELY}(s) = R_{ELY} \times \frac{K_{ELY}}{T_{ELY}s+1} = \frac{P_{ELY}^{rated}}{P_{sys}^{rated}} \times \frac{K_{ELY}}{T_{ELY}s+1} \quad (5)$$

where R_{ELY} represents the ratio of the electrolyser plant rated power (P_{ELY}^{rated}) to the total grid power (P_{sys}^{rated}), while K_{ELY} and T_{ELY} are the numerator and denominator of the first order transfer function, and can be calculated based on the value and definition of rise time, and settling time, using Eq. (6).

3. Modelling of Electrolyser Plant

3.1. Power-Tracking Response Characteristic

In [3], experiments are carried out, in which the overall ramp-up and ramp-down characteristics of PEM and alkaline electrolysis stack are evaluated. These characteristics can be quantified as the initial response time (T_{ini}), the rise time (T_r), and the settling time (T_s), which are defined as the time it takes for the electrolyser current to reach 1%, 50%, and 95% of the reference signal, respectively [12] [3]. The PEM electrolyser has a faster response to the reference signal, compared to the alkaline electrolyser. Thus, the initial response time, rise time, and settling time of the PEM electrolyser are lower than that of the alkaline electrolyser. These three parameters are critical to simulate the power-tracking response characteristic of PEM and the alkaline electrolyser, which is displayed as the first-order transfer function $G_{ELY}(s)$ using Eq. (5). Based on the step response method as shown in Eq. (6), the transfer function parameters K_{ELY} and T_{ELY} can be identified.

$$\begin{cases} P_{ELY}(\infty) - \left[P_{ELY}(\infty) - P_{ELY}(0)\right] \times e^{\frac{T_r}{T_{ELY}}} = 50\% \\ P_{ELY}(\infty) - \left[P_{ELY}(\infty) - P_{ELY}(0)\right] \times e^{\frac{T_s}{T_{ELY}}} = 95\% \end{cases} \quad (6)$$

where $P_{ELY}(\infty)$ (p.u) and $P_{ELY}(0)$ (p.u) is the consumed power of the electrolyser in steady-state ($t = \infty$), and when $t = 0$. The $P_{ELY}(0)$, in this case, is equal to 0. The rise time and settling time for the PEM electrolyser plant are selected to be 0.02 and 0.06 seconds, respectively, while the rise time and settling time for the alkaline electrolyser plant are 1 and 4 seconds, according to [12]. This results in K_{ELY} = 1.1693 and T_{ELY} = 0.0358 for the PEM electrolyser plant and K_{ELY} = 1.0184 and T_{ELY} = 1.4809 for the alkaline electrolyser plant. In addition, the initial response time is set to be 0.013 seconds for the PEM electrolyser and 0.019 seconds for the alkaline electrolyser, according to [3].

3.2. Proposed Droop and Virtual Inertia Controller

This study uses an active power-frequency droop characteristic, as shown in Figure 3, which takes into account the electrolyser initial operating point (P_{ini}), its maximum and minimum power (P_{max}, P_{min}), as well as the upper and lower power bounds (P_{upper}, P_{lower}) of the droop controller.

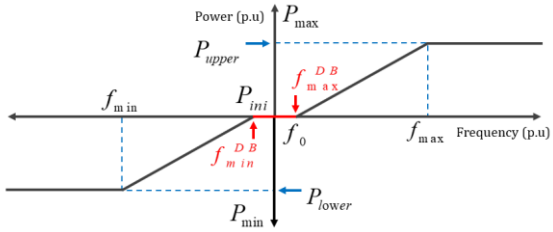

Figure 3 Active P-f droop characteristic of electrolyser plant

Based on the proposed droop controller, the electrolyser plant is able to provide both upward and downward frequency control if it is not operating at its maximum or minimum power, and the system frequency is within the regulation band ($\Delta f \in [f_{min}; f_{min}^{DB}] \cup [f_{max}^{DB}; f_{max}]$). The electrolyser plant reference power consumption can be calculated as:

$$P_{ELY} = \begin{cases} \min\left(P_{upper}; P_{\max}\right) \text{ if } f > f_{\max} \\ \max\left(P_{lower}; P_{\min}\right) \text{ if } f < f_{\min} \\ D_{ELY} f \text{ if } \left[f_{\min}; f_{\max}^{DB}\right] < f < \left[f_{\min}^{DB}; f_{\max}\right] \\ 0 \quad \text{if } f_{\min}^{DB} < f < f_{\max}^{DB} \end{cases} \quad (7)$$

According to Eq. (7), the electrolyser plant would perform a linear P-f characteristic within the range [f_{min}; f_{max}]. When the system frequency is larger than the maximum frequency or lower than the minimum frequency, the electrolyser plant will operate at constant power, equal to P_{upper} and P_{lower}, respectively. These two values could equal, lower, or higher than P_{max} and P_{min}, depending on the given droop coefficient and initial operating point.

In addition to the proposed droop controller, this study also considers the ability to provide virtual inertia of the electrolyser plant. Electrolyser plants with the ability to provide VIC allow themselves to synchronise with the external grid without relying heavily on its features and characteristics [17]. As a result, their synchronisation is much better than that of a grid-following electrolyser plant, which is more sensitive to changes in external system conditions. The virtual inertia effect is added to the electrolyser plant dynamic behaviour and can be adjusted by regulating the virtual inertia coefficient (H_{vir}) [12]. The larger the H_{vir} value is, the more virtual inertia response the electrolyser plant is able to provide.

3.3. Reference Power Generation Strategies

Based on the proposed controllers above, three different control strategies have been utilised, including (1) the droop controller, (2) the Rate Of Change Of Frequency (RoCoF)-based droop controller, and (3) the RoCoF-based droop controller and VIC (Figure 4). The first strategy only utilises a typical droop controller without considering the impact of virtual inertia control of the electrolyser plant or any other advanced controller. The RoCoF-based droop controller, besides having the same P-f droop characteristic as the first strategy, also considers the impact of the RoCoF using the control coefficient C. By adjusting this parameter, the impact of the RoCoF on the reference electrolyser plant power would either increase or decrease, as shown in Figure 4. In scenarios when the system is witnessing an extreme RoCoF, the second

control strategy will allow the electrolyser plant to have a more substantial frequency response by increasing or decreasing the consumption power more significantly. The third strategy utilises both the RoCoF-based droop controller and the VIC to further improve the system frequency response. By adjusting the parameters H_{vir} and C, the system frequency response might be improved. However, it should be noted that although the frequency nadir of the system might be improved by increasing these controller parameters, the settling time would also increase. Because of that, optimal methods should be applied when calculating controller parameters.

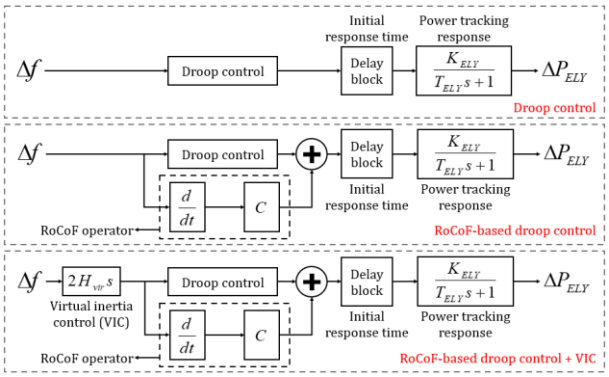

Figure 4 Electrolyser plant power reference generation strategies

4. Modified SFR Model Parameter Estimation and Validation

4.1. *Parameter Estimation*

Using the system dynamic frequency response and power disturbance obtained from real system data or detailed models as references, the transfer function $G_m(s)$ parameters can be identified using PSO. The objective function for the fitting process is presented as follows:

$$RMSE = \sqrt{\frac{1}{n}\sum_{i=1}^{n}\left(\Delta f_i - \widetilde{\Delta f}_i\right)^2} \quad (8)$$

where n is the number of considered frequency response data points, $\Delta \boldsymbol{f_i}$ is the actual frequency response data or obtained from a detailed model, and $\widetilde{\Delta \boldsymbol{f_i}}$ is the frequency response data obtained from the proposed SFR model.

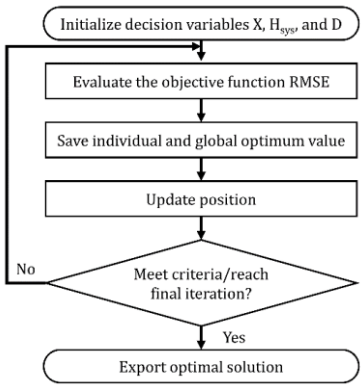

Figure 5 Optimisation flowchart for the estimation process

The PSO algorithm, inspired by the flight behaviour of groups of birds in search of food, utilises a large number of particles that constitute a swarm moving around in the search space, following a specific rule, to find the best solution. The particles mentioned are the decision variable X, which includes [x_1, x_2, x_3, x_4, x_5, x_6], H_{sys}, and D, and the best solution is defined as a solution with the lowest RMSE. The optimisation flowchart to estimate the parameters of the modified SFR model is shown in Figure 5, while the estimated parameters and errors are listed in Table 1 and Table 2, respectively.

Table 1 Estimated parameters of the modified SFR model

Parameters	**H**	**D**	**[x_1; x_2; x_3; x_4; x_5; x_6]**
Estimation	2.61	0	[5475.35; 3561.66; 17.66; 467.36; 1021.17; 228.10]

4.2. *Fitting Capability Validation*

The fitting capability of the PSO algorithm is tested using a modified IEEE 39-bus system with 50% wind turbine penetration, simulated in the PSS/E software. The reference frequency response is obtained by creating a disturbance of a 10% load increase at bus 27 in PSS/E, while the modified SFR model adjusts its parameters to fit its generated frequency response with the reference value. Besides the RMSE value of the reference and the fitted frequency response, other evaluation criteria, including mean absolute error (MAE) and mean absolute percentage error (MAPE), are also calculated. The three evaluation errors are given in Table 2. It can also be seen in Figure 6 that the PSO algorithm is able to find the optimal parameters that allow the modified SFR model to produce frequency responses that are highly similar to the reference value. The frequency nadir and steady-state frequency in the three cases are accurately identified. In addition, the parameters generated for one scenario can be applied to other scenarios with high accuracy, which is in this case, the parameters for the 10% load increase scenario are used in 7.5% and 5% load increase scenarios.

Table 2 Errors of the modified SFR model

Error	**RMSE [Hz]**	**MAPE [%]**	**MAE [Hz]**
10% load increase	6.89×10^{-5}	0.9676	3.76×10^{-5}
7.5% load increase	1.86×10^{-4}	2.1977	1.03×10^{-4}
5% load increase	1.58×10^{-4}	3.1386	1.01×10^{-4}

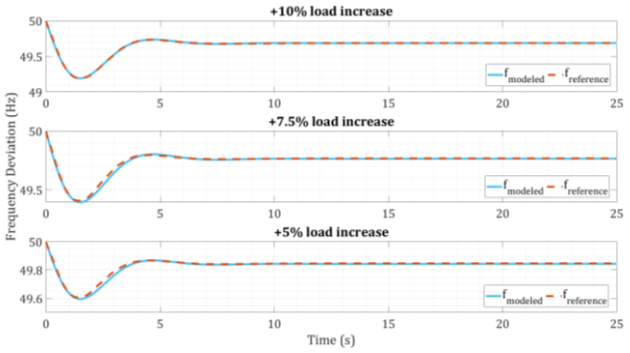

Figure 6 Comparison of the modified SFR model and PSS/E frequency response model

5. Case Studies

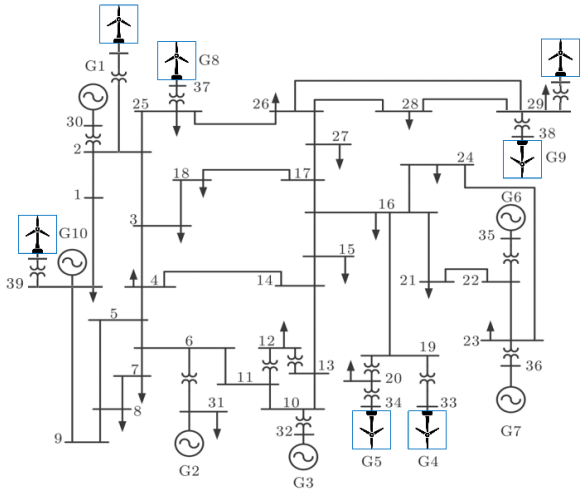

Figure 7 The modified IEEE 39-bus system with 50% wind turbine penetration

This section analyses different cases demonstrating the capability of providing frequency support of the PEM and alkaline electrolyser plant after an extreme disturbance (10% increase in load demand). In addition, different control strategies, including typical droop control, RoCoF-based droop control, and virtual inertia control, are also evaluated. For the case study, this paper uses the IEEE 39-bus system, representing the simplified New England power grid in the United States. The original system consists of 10 synchronous generators, all equipped with devices such as governors and excitation systems. The system is then modified by connecting large-scale wind turbines in buses 2, 29, 33, 34, 37, and 37 to 39, as shown in Figure 7. The SGs' installed capacity is 2902 MW, while the added wind turbines' capacity is 3000 MW, making the wind turbine penetration rate in the system 50.83%. The grid-scale PEM/Alkaline electrolyser plant is then integrated into the modified IEEE 39-bus power system, to evaluate its ability to support the system frequency stability. The simulation is conducted in MATLAB/SIMULINK, using the given values and estimated parameters in Table 1 and Table 3. The following cases are evaluated:

- Base case: No electrolyser in the system
- Case 1: 1 GW PEM electrolyser plant with droop controller
- Case 2: 1 GW PEM electrolyser plant with RoCoF-based droop controller
- Case 3: 1 GW alkaline electrolyser plant with RoCoF-based droop controller
- Case 4: 1 GW PEM electrolyser plant with RoCoF-based droop controller and VIC

Table 3 The parameters used in the modified SFR model

Parameters	**Value**	**Unit**
Nominal frequency (f_{nom})	50	Hz
Frequency range (f_{min}-f_{max})	49.5-50.5	Hz
Frequency deadband (f_{min}^{DB}- f_{max}^{DB})	49.985-50.015	Hz
Droop coefficient (D_{ELY})	100	-
RoCoF control coefficient (C)	100	-
Electrolyser virtual inertia (H_{vir})	5	s
Capacity ratio (R_{ELY})	16.9	-
Electrolyser initial power (P_{ini})	1000	MW

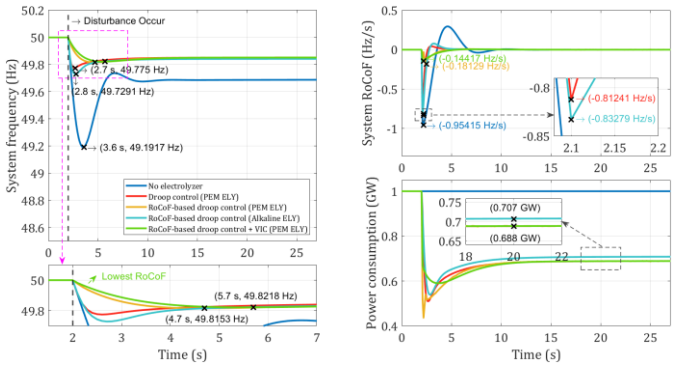

Figure 8 System frequency, RoCoF, and electrolyser plant consumed power under five scenarios

In the modelled cases shown in Figure 8, the initial operating power of the electrolyser plant is set equal to 1 p.u. The disturbance occurs at 2 seconds, decreasing the power system frequency (with no electrolyser) in the base case down to 49.19 Hz after 1.6 s, and generating the largest RoCoF value of 0.95 Hz/s. By applying a basic droop control to the 1 GW PEM electrolyser plant, the system frequency nadir witnesses a significant increase in value, from 49.19 Hz (base case) to 49.78 Hz in 0.7 s in case 1. This significant increase in frequency nadir results from the rapid response of the 1 GW PEM electrolyser plant to the frequency drop in just a fraction of a second, reducing its consumed power by around 50%. The system RoCoF is also reduced to 0.81 Hz/s, and the steady-state frequency is also improved from 49.69 Hz to 49.85 Hz.

In case 2, the basic droop control is improved by considering the impact of RoCoF, using the RoCoF coefficient C. The frequency nadir, in this case, is further increased by 0.04 Hz, compared to case 1 (from 49.78 Hz to 49.82 Hz). It should be noted that compared to the previous scenarios (base case and case 1), case 2 has a significantly lower RoCoF, with only 0.18 Hz/s, instead of 0.95 Hz/s in the base case and 0.81 Hz/s in case 1. This is due to the impact of the RoCoF-based droop control, which ensures a larger electrolyser plant consumed power decrease, compared to the droop control case. Thus, the consumed power of the electrolyser plant in this case also falls more significantly, down by 58%, instead of 50% in case 1.

In case 3, a 1 GW alkaline electrolyser plant is utilised for system frequency support, instead of PEM electrolyser. Although using the RoCoF-based droop control, the alkaline electrolyser plant is unable to increase the frequency nadir and RoCoF, compared with cases 1 and 2, and even worsens it. The frequency nadir and RoCoF in this case are 49.73 Hz and 0.83 Hz/s, respectively. This can be explained by the fact that the alkaline electrolyser plant has a much slower response compared to the PEM electrolyser plant, as discussed in Section 3.1, which results in a slower change in consumed power when the system frequency varied. Additionally, the studied system is also operating in low-inertia conditions with

more than 50% wind turbine penetration, thus increasing the RoCoF values significantly after the disturbance occurs.
In case 4, the full controller, including RoCoF-based droop control and VIC, is used. It can be noticed that besides improving frequency nadir and RoCoF to their best values in all cases (49.82 Hz and 0.14 Hz/s), the full controller also allows a less significant decrease in the electrolyser plant power in the first few seconds after the disturbance occurs. The maximum decrease in consumed power is reduced to only 41%, instead of 58% in case 2.

6. Conclusion

This study investigates the frequency support capability of a grid-scale electrolyser plant in a high wind penetration power system. A universal system frequency response model, derived from a full-order transfer function model, that ensures high accuracy, low computation time, and low required parameters is proposed. From there, different control strategies are introduced, including conventional droop control, RoCoF-based droop control, and virtual inertia control. In addition, the power-tracking response ability of different electrolyser types, including PEM and alkaline electrolysers, is evaluated. Utilising the modified IEEE 39-bus with 50% wind penetration, the proposed control strategies have proved their performance in providing better frequency response after an extreme disturbance. The RoCoF-based droop control even showed its capability by greatly decreasing the maximum RoCoF, compared with the conventional droop controller. Finally, the slow response characteristic of the alkaline electrolyser plant has been shown to negatively impact its capability to provide frequency support to power systems. Future work will focus on designing optimal control strategies, that are based on advanced algorithms, to further improve the frequency response of power systems. Other technical aspects of the electrolyser plant, including overloading capability, and hydrogen buffer constraints, will also be looked at. Additionally, the economic aspects of electrolyser plants that provide frequency support services will also be considered to evaluate their profitability.

Acknowledgment

This research has been funded by OWC, ABL Group. The authors are grateful for such financial support as well as technical discussion and input from OWC experts including Piotr Jedrzejewski (for reviewing the paper) and Riccardo Felici (for providing resources).

References

[1] IRENA, "Renewable capacity highlights," 2023.

[2] H. Evelyn, T. Fei and S. Goran, "Challenges and opportunities of inertia estimation and forecasting in low-inertia power systems," *Renewable and Sustainable Energy Reviews,* 2021.

[3] J. Eichman, K. Harrison and M. Peters, "Novel Electrolyzer Applications: Providing More Than Just Hydrogen," NREL, 2014.

[4] P. Guangsheng, G. Wei, L. Yuping, Q. Haifeng, L. Shuai and Y. Shuai, "Optimal Planning for Electricity-Hydrogen Integrated Energy System Considering Power to Hydrogen and Heat and Seasonal Storage," *IEEE Transactions on Sustainable Energy,* 2020.

[5] N. Nur Dalilah and R. Hasimah Abdul, "Comparison of optimum design, sizing, and economic analysis of standalone photovoltaic/battery without and with hydrogen production systems," *Renewable Energy,* 2019.

[6] V. Long Phan, C. Kien Do and D. Tuyen Nguyen, "Review of hydrogen technologies based microgrid: Energy management systems, challenges and future recommendations," *International Journal of Hydrogen Energy,* 2023.

[7] V. Long Phan, H. Long Hoang, C. Kien Do, T. Hirotaka and D. Tuyen Nguyen, "An improved state machine-based energy management strategy for renewable energy microgrid with hydrogen storage system," *Energy Reports,* 2023.

[8] D. Van Nguyen, L. Paul, M. Eamon, M. Jimmy and C. Val, "Development of a viability assessment model for hydrogen production from dedicated offshore wind farms," *International Journal of Hydrogen Energy,* 2021.

[9] D. Quang Vu, D. Van Nguyen, M. Hadi, P. Pedro H. Todesco and L. Paul G., "A geospatial method for estimating the levelised cost of hydrogen production from offshore wind," *International Journal of Hydrogen Energy,* 2023.

[10] D. Mehdi Ghazavi, J. Ahvand and M. Pierluigi, "Fast Frequency Response From Utility-Scale Hydrogen Electrolyzers," *IEEE Transactions on Sustainable Energy,* 2021.

[11] D. Mehdi Ghazavi, C. Antonella Maria De and M. Pierluigi, "Fast Frequency Response Provision from Large-Scale Hydrogen Electrolyzers Considering Stack Voltage-Current Nonlinearity," in *2021 IEEE Madrid PowerTech. IEEE,* Madrid, 2021.

[12] D. Mehdi Ghazavi, C. Antonella Maria De and M. Pierluigi, "Virtual Inertia Response and Frequency Control Ancillary Services From Hydrogen Electrolyzers," *IEEE Transactions on Power Systems,* 2022.

[13] H. Chunjun, Z. Yi, Y. Shi and T. Chresten, "Analytical Modeling and Control of Grid-Scale Alkaline Electrolyzer Plant for Frequency Support in Wind-Dominated Electricity-Hydrogen Systems," *IEEE Transactions on Sustainable Energy,* 2022.

[14] H. Md. Biplob, I. Md. Rabiul, M. Kashem M., S. Danny and A. Ashish P., "Power System Dynamic Performance Analysis Based on Frequency Control by Proton Exchange Membrane Electrolyzers," *IEEE Transactions on Industry Applications,* 2023.

[15] S. Hadi, Power System Analysis, McGraw-Hill, 1999.

[16] H. Huang, P. Ju, Y. Jin, X. Yuan, C. Qin, X. Pan and X. Zang, "Generic System Frequency Response Model for Power Grids With Different Generations," *IEEE Access,* 2020.

[17] D. Mehdi Ghazavi and M. Pierluigi, "Frequency Stability Supports from Battery Storage with Virtual Synchronous Machine Control," in *2021 IEEE PES Innovative Smart Grid Technologies-Asia*, 2021.